

Community-based benchmarking improves spike inference from two-photon calcium imaging data

Philipp Berens^{1,2,3}, Jeremy Freeman⁴, Thomas Deneux⁵, Nicolay Chenkov⁶, Thomas McColgan⁶, Artur Speiser⁷, Jakob H. Macke⁷, Srinivas C. Turaga⁸, Patrick Mineault⁹, Peter Rupprecht^{10,11}, Stephan Gerhard¹⁰, Rainer W. Friedrich^{10,11}, Johannes Friedrich¹², Liam Paninski¹², Marius Pachitariu¹³, Kenneth D. Harris¹³, Ben Bolte¹⁴, Timothy A. Machado¹², Dario Ringach¹⁵, Jacob Reimer^{16,17}, Emmanouilis Froudarakis^{16,17}, Thomas Euler^{1,2,3}, Miroslav Román Rosón^{1,2,18,19}, Lucas Theis²⁰, Andreas S. Tolias^{16,17,21}, & Matthias Bethge^{2,3,22}

¹*Institute for Ophthalmic Research, University of Tübingen, Tübingen, Germany*

²*Center for Integrative Neuroscience, University of Tübingen, Tübingen, Germany*

³*Bernstein Center for Computational Neuroscience, University of Tübingen, Tübingen, Germany*

⁴*Chan Zuckerberg Initiative, San Francisco, USA*

⁵*Unit de Neurosciences, Information et Complexité, Centre National de la Recherche Scientifique, Gif-sur-Yvette, France*

⁶*Bernstein Center for Computational Neuroscience and Institute for Theoretical Biology, Humboldt-Universität zu Berlin, Berlin, Germany*

⁷*research center caesar, an associate of the Max Planck Society, Bonn, Germany*

⁸*Janelia Research Campus, Howard Hughes Medical Institute, Ashburn, Virginia, USA*

⁹*Independent Researcher*

¹⁰*Friedrich Miescher Institute, Basel, Switzerland*

¹¹*University of Basel, Basel, Switzerland*

¹²*Departments of Statistics and Neuroscience, Grossman Center for the Statistics of Mind, and Center for Theoretical Neuroscience, Columbia University, New York, NY, USA*

¹³*University College, London, UK*

¹⁴*Emory University, Atlanta, USA*

¹⁵*University of California, Los Angeles, CA, USA*

¹⁶*Department of Neuroscience, Baylor College of Medicine, Houston, TX, USA*

¹⁷*Center for Neuroscience and Artificial Intelligence, Baylor College of Medicine, Houston, TX, USA*

¹⁸*Graduate School of Neural & Behavioural Sciences, International Max Planck Research School, University of Tübingen, Tübingen, Germany*

¹⁹*Division of Neurobiology, Department Biology II, LMU Munich, Munich, Germany*

²⁰*Twitter, London, UK*

²¹*Department of Electrical and Computer Engineering, Rice University, Houston, TX, USA*

²²*Institute of Theoretical Physics, University of Tübingen, Tübingen, Germany*

In recent years, two-photon calcium imaging has become a standard tool to probe the function of neural circuits and to study computations in neuronal populations^{1,2}. However, the acquired signal is only an indirect measurement of neural activity due to the comparatively slow dynamics of fluorescent calcium indicators³. Different algorithms for estimating spike trains from noisy calcium measurements have been proposed in the past⁴⁻⁸, but it is an open question how far performance can be improved. Here, we report the results of the *spikefinder* challenge, launched to catalyze the development of new spike inference algorithms through

crowd-sourcing. We present ten of the submitted algorithms which show improved performance compared to previously evaluated methods. Interestingly, the top-performing algorithms are based on a wide range of principles from deep neural networks to generative models, yet provide highly correlated estimates of the neural activity. The competition shows that benchmark challenges can drive algorithmic developments in neuroscience.

We organized the *spikefinder* challenge to crowd-source the problem of developing algorithms for inferring spike rates from calcium signals. Such challenges have been used successfully in machine learning and computer vision to drive algorithmic developments⁹. We used a benchmark data set consisting of 92 recordings from 73 neurons⁶, acquired in the primary visual cortex and the retina of mice using different calcium indicators (OGB-1 and GCaMP6s), different scanning methods, and different sampling rates. For this data, calcium imaging has been performed simultaneously with electrophysiological recordings allowing to evaluate the performance of spike inference algorithms on ground truth data. Importantly, all data has been acquired at a zoom factor typically used during population imaging experiments, ensuring that all benchmark results reflect performance under the typical use-case conditions.

For the challenge, we split the data into a training and a test set (see Table 1). For the training data, we made both the calcium and the spike traces publicly available, but kept the spike traces secret for the test data. Additionally, the publicly available data sets provided by the GENIE project¹⁰ were available as training data. This allowed participants to adjust their models on the training data set, while avoiding overfitting to the specific benchmark data set. Participants could

upload predictions for the spike rate generated by their algorithm on a dedicated website (see Methods) and see their performance on the training set during the competition phase. Results on the test set were not accessible to the participants during the competition. To evaluate the quality of the prediction, we computed the Pearson correlation coefficient between the true spike trace and the prediction sampled at 25 Hz (equivalent to 40 ms time bins) as previously described⁶.

We obtained 37 submissions, from which we selected all algorithms performing better than the STM algorithm, which had previously been shown to outperform other algorithms on this data⁶. In addition, if there were multiple submissions from the same group, we used the one with the highest correlation on the test set. This resulted in a total of ten algorithms that we studied in greater detail (see Table 2). Interestingly, these submissions include algorithms based on very different principles: some of the algorithms built on the classical generative models of spike-induced calcium dynamics⁴, while others relied on purely data-driven training of deep neural networks or pursued hybrid strategies (see Table 3).

We found that several of the submitted algorithms performed substantially better than the STM, increasing the average correlation on the test set from 0.36 by 0.08 to 0.44 for the best algorithm (Figure 1A, B; Table 3). Because increases in correlation are hard to interpret, we converted it to mutual information assuming a Gaussian distribution (see Methods), yielding an estimated increase of almost 50% on average. For all algorithms, performance varied substantially between data sets with the best results observed on data set I. Interestingly, performance gains were typically larger on GCaMP6 than on OGB-1 data sets (Figure 1B). Surprisingly, the top group

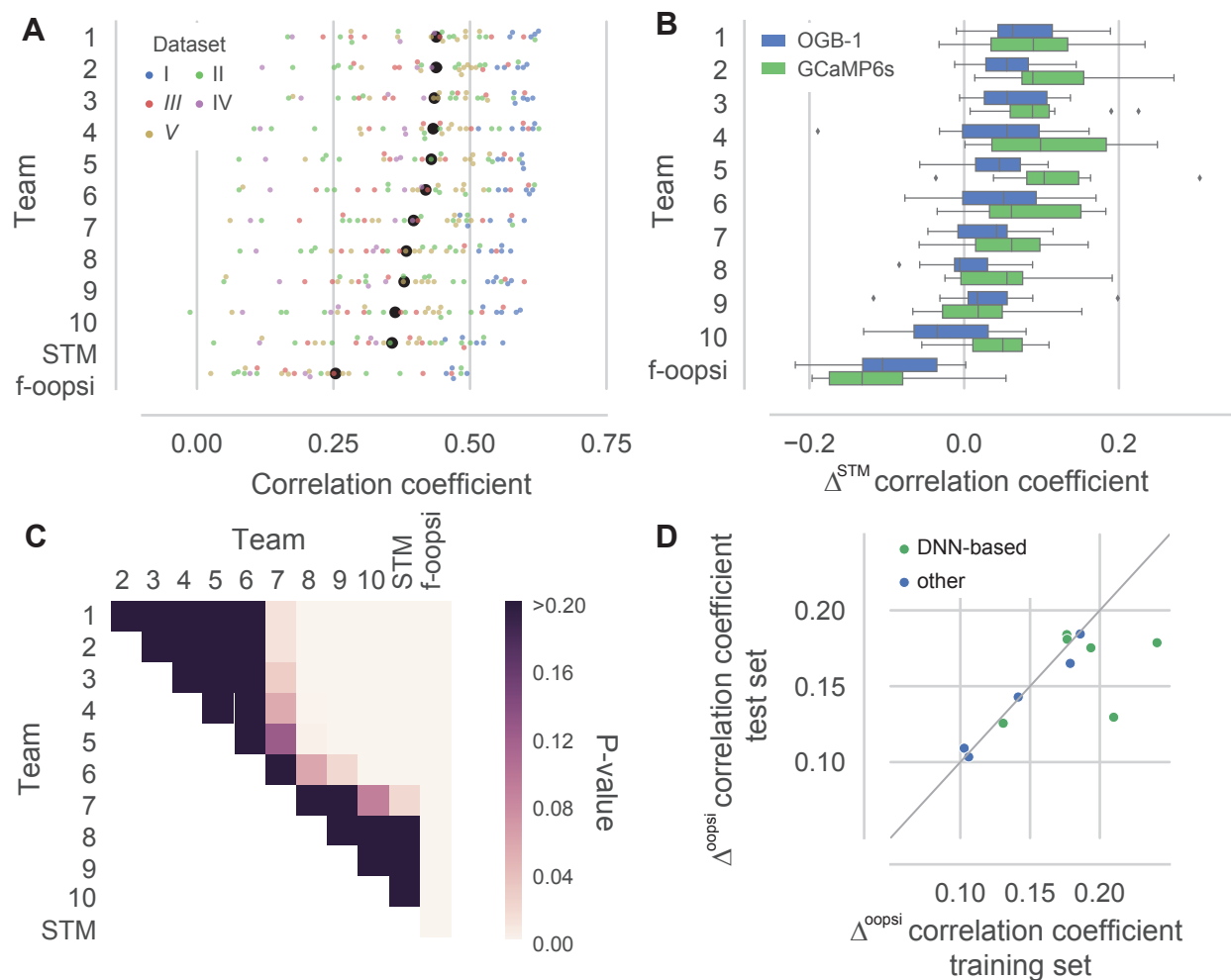


Figure 1: Contributed algorithms outperform state-of-the-art. **A**. Correlation coefficient of the spike rate predicted by the submitted algorithms (evaluated at 25 Hz, 40 ms bins) on the test set. Colors indicate different data sets (for details, see Table 1). Data sets I, II, and IV were recorded with OGB-1 as indicator, III and V with GCaMP6s. Black dots are mean correlation coefficients across all $N = 32$ cells in the test set. Colored dots are jittered for better visibility. STM: Spike-triggered mixture model⁶; f-oopsi: fast non-negative deconvolution¹¹ (*continued next page*)

Figure 1: (continued from previous page) **B.** Difference in correlation coefficient on the test set to the STM, split by the calcium indicator used in the data set. **C.** P-values for difference in mean correlation coefficient on the test set for all pairs of algorithms (Repeated measured ANOVA, $N = 32$ cells, main effect of algorithm: $P < 0.001$, shown are p-values for post-hoc pairwise comparisons, corrected using Holm-Bonferroni correction) **D.** Difference in correlation coefficient split by algorithm type on the training and test set, respectively, to the f-oopsi-result correcting for systematic differences between the training and the test set.

of six algorithms performed virtually indistinguishably (Figure 1C), despite using very different methodologies. Finally, we evaluated to what extent the algorithms overfitted the training data. For example, it is possible that algorithms extracted peculiarities of the training data that did not transfer to the test data, resulting in artificially high correlation coefficients on the training data. We found that most algorithms showed similar performance for both the training and the test set, with evidence for overfitting in some of the DNN-based algorithms (Figure 1D).

As the algorithms in the top group used a range of algorithmic strategies, we wondered whether they also made different predictions, e.g., each capturing certain aspects of the spike-calcium relationship. However, the predictions of the different algorithms are typically very similar with an average pairwise correlation coefficient among the first six algorithm of $0.82 \pm .04$ (mean \pm SD, Figure 2). Also, averaging the top six predictions in an ensembling approach did not yield substantially better performance ($\bar{c} = 0.4436$ compared to $\bar{c} = 0.4382$ for Team 1). This indicates that despite their different algorithmic strategies, all algorithms capture similar aspects

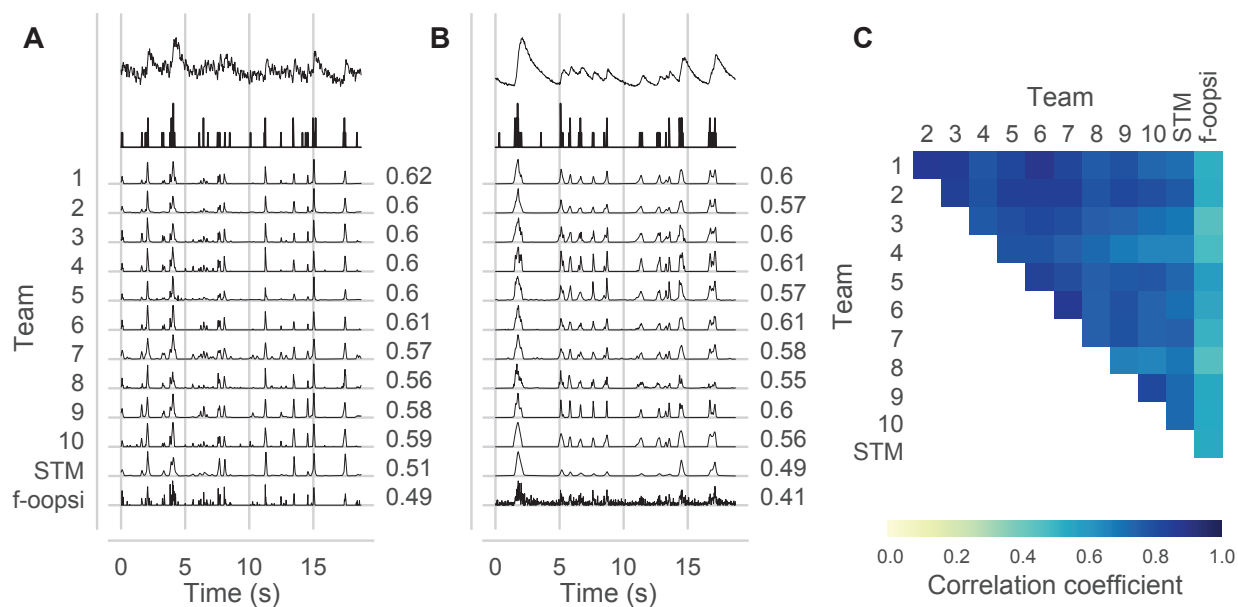


Figure 2: Top algorithms make highly correlated predictions. **A.-B.** Example cells from the test set for dataset 1 (OGB-1) and dataset 3 (GCaMP6s) show highly similar predictions between most algorithms. **C.** Average correlation coefficients between predictions of different algorithms across all cells in the test set at 25 Hz (40 ms bins).

of the spike-fluorescence relationship.

In summary, the *spikefinder* challenge has shown that a community competition making use of suitable benchmark data can catalyze algorithmic developments in neuroscience. The challenge triggered a range of new and creative approaches towards solving the problem of spike inference from calcium data and improved the state-of-the-art substantially. Interestingly, the challenge did not distill the optimal strategy out of the different possible algorithmic approaches, something we had initially hoped for; rather, it showed that – given the current data – a range of approaches yield

very similar outcomes. In particular, it is noteworthy that algorithms based on generative models such as those by Team 1 and 6 perform on par with more flexible deep learning-based approaches. Each algorithm comes with their own advantages and disadvantages regarding speed, interpretability, and incorporation of prior knowledge. For example, training the DNN-based models is computationally quite costly, and care has to be taken when using complex DNN-based models to avoid overfitting the training set, as this could lead to false confidence about the prediction performance on new data. On the other hand, the DNN-based approaches are less reliant on prior knowledge and may be more easily adapted when new training data sets are acquired with new indicators with different dynamics. In contrast, the algorithms based on generative models allow for very fast inference (Team 6) or Bayesian treatment (Team 1), but may be less easily adapted to novel settings.

More generally, the *spikefinder* challenge raises the question of what the actual performance bound of an ideal decoder is. Model simulations can help to answer these questions^{7,12}, but their interpretation is limited by the accuracy of the model regarding indicator dynamics, noise structure, and other experimental factors⁶. However, the challenge contributions by Team 9 and a recent paper¹³ by Team 3 have shown that they can actually be useful for training supervised algorithms. It remains to be seen whether new and larger data sets of simultaneously recorded and imaged neurons will yield further improvements and distinguish more clearly between different algorithmic strategies. It will also be interesting to see whether new indicators will allow for more precise spike-rate inference.

In addition to improving on the state-of-the-art, competitions such as the *spikefinder* challenge can boost standardization of algorithms, something that has been lacking from neuroscience analysis tool chains¹⁴. During and after the challenge, lively debates ensued online about the best way to handle several of the processing steps highlighting several potential pitfalls in analyzing calcium imaging data. Some of these difficulties were also reflected in the choices made for this challenge. For example, we resampled all data to 100 Hz for ease of comparison, which induced problems for some of the participating algorithms through the properties of the used filter. In addition, several of the participating teams found it necessary to introduce means of adapting the model parameters to the specific data set as, e.g., the average time delay between the spike and calcium signal seemed to vary between data sets. This may be due to different preprocessing procedures performed in the different data sets, but such confounds should be avoided in future competitions on this topic. Finally, the challenge was performed on traces extracted from the raw imaging data by averaging all the pixels within manually placed regions-of-interest (ROIs). It is thus possible that the extracted signals contain contamination from the neuropil or were suboptimally placed, a problem tackled by methods that combine ROI placement and calcium-trace extraction in a single algorithm^{5,15}. However, at least for data with simultaneous imaging and electrophysiological recordings, it is not clear how methods integrating ROI placement and spike-rate extraction should be evaluated and compared to regular data, since the recording electrode is always present in the picture.

Alternatives to our primary evaluation measure, the correlation coefficient, may also need to be considered. While it is easy to interpret and more sensitive than the often used AUC-score, it is

still invariant under global scaling of the predicted spike rate⁶. In fact, different metrics can lead to different conclusions about which algorithm is optimal since the metric contains part of the task specification¹⁶. On the other hand, information gain – which may be considered a canonical model comparison criterion for probabilistic predictions^{6,17} – is considered less intuitive by some.

We believe that quantitative benchmarks are an essential ingredient for progress in the field, providing a reference point for future developments and a common standard with regards to how new algorithms should be evaluated. We strongly believe that many fields of computational neuroscience can benefit from community-based challenges to assess where the field stands and how it should move forward. As for the problem of spike inference from two-photon imaging, the *spikefinder* challenge should not be considered the last word in this matter: More comprehensive data sets and new functional indicators may require organizing another round of community-based development, further pushing the boundaries of what is attainable.

Methods

Data The challenge was based on data sets collected for a previous benchmarking effort⁶ and the publicly available cai-1 data set from crcns.org¹⁰. Details about the recording region, indicators, scan rate and cell numbers are summarized in Table 1. All data was resampled to 100 Hz independent of the original sampling rate. Upon request during the challenge, we made the data available at the native sampling rate.

Challenge organization For the challenge, we split the available data into training and test sets (see Table 1). The training set contained both calcium and spike data, while for the test set, only calcium data was available during the challenge period. The GENIE datasets were only used as training data, since they are completely publicly available and consist of recordings from individual zoomed-in cells.

The data and instructions were available on a dedicated website, based on an open-source web framework (<https://github.com/codeneuro/spikefinder>). There was a discussion board linked from the website to allow for questions and discussion among participants. Each team could make multiple submissions, but during the challenge period, only results on the training set were shown. The challenge ran from 30/11/2016 to 04/05/2017.

Algorithms The submitted algorithms are described in detail in the Supplementary Information. For comparison, we used publicly available implementations of the STM algorithm⁶ and fast-opsi¹¹. STM parameters were optimized on the training set.

Evaluation The evaluation of the submissions was done in Python using Jupyter notebooks. All notebooks are available at https://github.com/berenslab/spikefinder_analysis. We used the correlation coefficient between the inferred and the real traces resampled to 25 Hz (40 ms time bins) as a quality measure. Because difference in correlation is hard to interpret (e.g., because an increase from .40 to .45 means something very different than an increase from .94 to .99), we converted correlation coefficients to information rate assuming a Gaussian channel:

$$I_{algo}^i = -\frac{1}{2} \log_2(1 - (c_{algo}^i)^2)$$

Improvements in performance were then computed as the increase in average information rate compared to the STM algorithm:

$$100 \cdot \left(\frac{\langle I_{algo}^i \rangle}{\langle I_{STM}^i \rangle} - 1 \right) \%$$

We used the R package `aFex` to compute a repeated measures ANOVA on the correlation coefficients with within-subject factor algorithm and cells as subjects. Pairwise comparisons between algorithms were performed using the `lsmeans` package with Holm-Bonferroni correction for 66 tests.

References

1. Kerr, J. N. & Denk, W. Imaging in vivo: watching the brain in action. *Nature Reviews Neuroscience* **9**, 195–205 (2008).
2. Peron, S., Chen, T.-W. & Svoboda, K. Comprehensive imaging of cortical networks. *Current Opinion in Neurobiology* **32**, 115–123 (2015).
3. Chen, T.-W. *et al.* Ultrasensitive fluorescent proteins for imaging neuronal activity. *Nature* **499**, 295–300 (2013).
4. Vogelstein, J. T. *et al.* Spike inference from calcium imaging using sequential Monte Carlo methods. *Biophysical journal* **97**, 636–55 (2009).
5. Pnevmatikakis, E. A. *et al.* Simultaneous denoising, deconvolution, and demixing of calcium imaging data. *Neuron* **89**, 285–299 (2016).
6. Theis, L. *et al.* Benchmarking Spike Rate Inference in Population Calcium Imaging. *Neuron* **90**, 471–482 (2016).
7. Deneux, T. *et al.* Accurate spike estimation from noisy calcium signals for ultrafast three-dimensional imaging of large neuronal populations in vivo. *Nature Communications* **7**, 12190 (2016).
8. Friedrich, J., Zhou, P. & Paninski, L. Fast online deconvolution of calcium imaging data. *PLoS Comput Biol* **13**, e1005423 (2017).

9. Russakovsky, O. *et al.* Imagenet large scale visual recognition challenge. *International Journal of Computer Vision* **115**, 211–252 (2015).
10. Svoboda, K. & Project, G. Simultaneous imaging and loose-seal cell-attached electrical recordings from neurons expressing a variety of genetically encoded calcium indicators (2015).
11. Vogelstein, J. T. *et al.* Fast nonnegative deconvolution for spike train inference from population calcium imaging. *Journal of neurophysiology* **104**, 3691–704 (2010).
12. Wilt, B., Fitzgerald, J. E. & Schnitzer, M. J. Photon shot noise limits on optical detection of neuronal spikes and estimation of spike timing. *Biophysical journal* **104**, 51–62 (2013).
13. Speiser, A., Turaga, S. & Macke, J. Upcoming. *arxiv* (2017).
14. Freeman, J. Open source tools for large-scale neuroscience. *Current Opinion in Neurobiology* **32**, 156–163 (2015).
15. Pachitariu, M. *et al.* Suite2p: beyond 10,000 neurons with standard two-photon microscopy. *bioRxiv* (2016). <http://www.biorxiv.org/content/early/2016/06/30/061507.full.pdf>.
16. Kummerer, M., Wallis, T. S. A. & Bethge, M. Saliency benchmarking: Separating models, maps and metrics. *arxiv* (2017). URL <https://arxiv.org/abs/1704.08615>.
17. Kummerer, M., Wallis, T. & Bethge, M. Information-theoretic model comparison unifies saliency metrics. *Proceedings of the National Academy of Science* **112**, 16054–16059 (2015).

18. Oord, A. v. d., Kalchbrenner, N. & Kavukcuoglu, K. Pixel recurrent neural networks. *arXiv preprint arXiv:1601.06759* (2016).
19. Kingma, D. P. & Welling, M. Auto-encoding variational bayes. *arXiv preprint arXiv:1312.6114* (2013).
20. Cho, K., Van Merriënboer, B., Bahdanau, D. & Bengio, Y. On the properties of neural machine translation: Encoder-decoder approaches. *arXiv preprint arXiv:1409.1259* (2014).
21. Glorot, X., Bordes, A. & Bengio, Y. Deep sparse rectifier neural networks. *Aistats* (2011).
22. He, K., Zhang, X., Ren, S. & Sun, J. Deep residual learning for image recognition. *arXiv* (2015). 1512.03385.
23. Abadi, M. *et al.* TensorFlow: Large-Scale machine learning on heterogeneous distributed systems. *arXiv* (2016). 1603.04467.
24. Graves, A. Generating sequences with recurrent neural networks. *arXiv* (2013). 1308.0850.
25. Otoro. Handwriting generation demo in TensorFlow. <http://blog.otoro.net/2015/12/12/handwriting-generation-demo-in-tensorflow/> (2015). Accessed: 2017-5-18.
26. Chollet, F. *et al.* Keras. <https://github.com/fchollet/keras> (2015).
27. Pedregosa, F. *et al.* Scikit-learn: Machine learning in Python. *Journal of Machine Learning Research* **12**, 2825–2830 (2011).

28. Friedrich, J. & Paninski, L. Fast active set methods for online spike inference from calcium imaging. In *Adv Neural Inf Process Syst* 29, 1984–1992 (2016).
29. Barlow, R. E., Bartholomew, D. J., Bremner, J. & Brunk, H. D. *Statistical inference under order restrictions: The theory and application of isotonic regression* (Wiley New York, 1972).
30. Pachitariu, M., Stringer, C. & Harris, K. D. Robustness of spike deconvolution for calcium imaging of neural spiking. *bioRxiv* 156786 (2017).
31. Jewell, S. & Witten, D. Exact spike train inference via l0 optimization. *arXiv:1703.08644* (2017).
32. van den Oord, A. *et al.* Wavenet: A generative model for raw audio. *CoRR abs/1609.03499* (2016).

Acknowledgements This work was funded by the German Ministry of Education and Research (BMBF; FKZ 01GQ1002 to MB, TE, AST; FKZ 01GQ1601 to PB), the German Research Foundation (EXC307, SFB1233 to MB, TE, PB, BE5601/1-1 to PB, SFB 1089 to JHM), the Wellcome trust (grants 108726, 95668, 95669 to KDH), the Swiss National Science Foundation (SNF; fellowship P300P2_158428 to JoF), the Boehringer Ingelheim Fonds (fellowship to PR), the Novartis Research Foundation, the Simons Foundation Global Brain Research Awards 325171, 325398, and 365002 (LP), the Army Research Office MURI (W911NF-12-1-0594, LP), the National Institutes of Health (NIH) BRAIN Initiative (R01EB22913, R21EY027592 to LP), the Defense Advanced Research Projects Agency (DARPA, N66001-15-C-4032, SIMPLEX to LP) and the National Institutes of Health (NEI, DP1 EY023176 to AST). In addition, this work was supported by the Intelligence Advanced Research Projects Activity (IARPA) via Department of Interior/ Interior Business Center (DoI/IBC) contract numbers D16PC00003 and D16PC00007 (LP, JR, AST, MB). The funders had no role in study design, data collection and analysis, decision to publish, or preparation of the manuscript. The U.S. Government is authorized to reproduce and distribute reprints for Governmental purposes notwithstanding any copyright annotation thereon. The views and conclusions contained herein are those of the authors and should not be interpreted as necessarily representing the official policies or endorsements, either expressed or implied, of IARPA, DoI/IBC, or the U.S. Government. Awards for the *spikefinder* competition were kindly provided by Carl Zeiss AG, Oberkochen, Germany and the Bernstein Center for Computational Neuroscience, Tübingen, Germany.

Author contributions PB, AST and MB designed the challenge; JeF provided web framework; PB and JeF ran the challenge; TD, NC, TM, AS, JHM, ST, PM, PR, SG, RF, JoF, LP, MP, KDH, TAM, DR submitted algorithms; JR, EF, TE, MRR, AST provided data; PB analyzed the results with input from MB; LT preprocessed data; PB wrote the paper with input from all authors.

Competing Interests The authors declare that they have no competing financial interests. The challenge was sponsored by Carl Zeiss AG with 2000 Euro.

Correspondence Correspondence and requests for materials should be addressed to P.B. (email: philipp.berens@uni-tuebingen.de).

Dataset	Indicator	Scan rate	N in training set	N in test set
I	OGB-1		11	5
II	OGB-1		21	10
III	GCamp6s		13	6
IV	OGB-1		6	3
V	GCamp6s		9	8

Table 1: Overview over datasets with training and test data used in the competition.

Team	Contributors
1	T. Deneux
2	N. Chenkov, T. McColgan
3	A. Speiser, J. Macke, S. Turaga
4	P. Mineault
5	P. Rupprecht, S. Gerhard, R. W. Friedrich
6	J. Friedrich, L. Paninski
7	M. Pachitariu
8	B. Bolte
9	T. Machado, L. Paninski
10	D. Ringach

Table 2: Reference table resolving team numbers to contributors

Team	Type	Note	train correlation	test correlation	Δ correlation	bits	Δ bits %
1	generative	Bayesian	0.4823	0.4382	0.0810	0.3077	56.2
2	supervised	DNN	0.4727	0.4378	0.0806	0.3070	55.9
3	supervised	DNN	0.4730	0.4347	0.0775	0.3022	53.5
4	supervised	DNN	0.5374	0.4325	0.0753	0.2987	51.7
5	supervised	DNN	0.4900	0.4291	0.0719	0.2936	49.1
6	generative	fast	0.4752	0.4188	0.0617	0.2783	41.3
7	generative		0.4379	0.3967	0.0395	0.2470	25.4
8	supervised	DNN	0.5063	0.3833	0.0261	0.2293	16.5
9	generative	GAN-style	0.4271	0.3794	0.0222	0.2242	13.9
10	supervised		0.3992	0.3629	0.0058	0.2038	3.5
STM	supervised		0.4024	0.3572		0.1969	
f-oopsi	generative		0.2964	0.2538	-0.1010	0.0961	-51.2

Table 3: Summary of main algorithm properties and performance. Δ correlation is computed as the mean difference in correlation coefficient compared to the STM algorithm. Δ bits in % is computed as the mean relative improvement in bits. All means are taken over $N = 32$ recordings in the test set, except for training correlation, which is computed over $N = 60$ recordings in the training set.

Supplementary Material

For all algorithms, we denote the spike train \mathbf{s} , the fluorescence trace \mathbf{f} and the underlying calcium signal \mathbf{c} , where applicable. We observe a total of T time bins, and the measurement in time bin t is written s_t , f_t and c_t , respectively.

Team 1 — T. Deneux The MLspike algorithm⁷ is a model-based Bayesian inference algorithm. Similarly to the method by Vogelstein et al.⁴, the conversion of neuronal spiking activity to calcium fluorescence is modeled by a biophysical dynamical system, and a two-ways filtering scheme is applied to estimate the hidden dynamics of the intracellular calcium concentration given the noisy fluorescence recording. MLspike implements two major improvements over previous models: The first one is an extension of the biophysical model including a slowly drifting baseline, which allows disentangling a wide range of noises often observed in the real data from the spike-related signals. The second one is to represent probabilities as dense arrays rather than using Monte-Carlo approximations, namely making MLspike a histogram filter instead of a particle filter, which improves both speed (at least for a models hidden state dimension not greater than 2) and accuracy.

For the spikefinder competition, MLspike was set to estimate a-posteriori probabilities $\mathbb{E}(s|c)$ rather than maximum-a-posteriori spike trains $\arg \max_s p(s|c)$. The biophysical model entailed a drifting baseline and nonlinear calcium to fluorescence conversion (i.e. saturation for OGB dataset; polynomial supralinearity for GCaMP6 dataset), and therefore had 6 or 7 parameters. One of these parameters (the a-priori spiking rate) was fixed while the 5 or 6 remaining ones

were estimated independently for each training dataset so as to maximize the match between the estimated and observed spikes. This was preferred to using MLspikes autocalibration method on each individual neuron, because the data appeared too noisy for this autocalibration to perform accurately. The match between spike trains was defined as the correlation after resampling to 25 Hz. We used an additional postprocessing optimization on the estimates consisting of temporal smoothing and a time shift to account for apparent differences between data sets. Once these optimizations were performed, the same model and postprocessing parameters were applied to the test data sets. Interestingly, the hyperparameter optimization strategy pursued here was very similar to that chosen by Team 6.

Code is available at <https://github.com/MLspike>.

Team 2 — N. Chenkov, T. McColgan This algorithm is based on a convolutional neural network, which receives the calcium signal and an index vector as input, denoting the data set the inputs come from. The network consists of eight convolutional layers and one recurrent layer (LSTM) (see Fig. 3A). We optimized the parameters by maximizing the Pearson correlation coefficient with the ground-truth spiking data at 25 Hz using the 'Adam' optimizer with 50 epochs.

The first layer consists of 10 units. Each unit uses a kernel with a width of 3 seconds (300 time steps) that is correlated with the input calcium signal. The learned kernels catch a basic repertoire of spike-related calcium dynamics (see Fig. 3A). The output of this layer is passed through a hyperbolic tangent activation function ('tanh'). This layer is followed by multiple convolutional

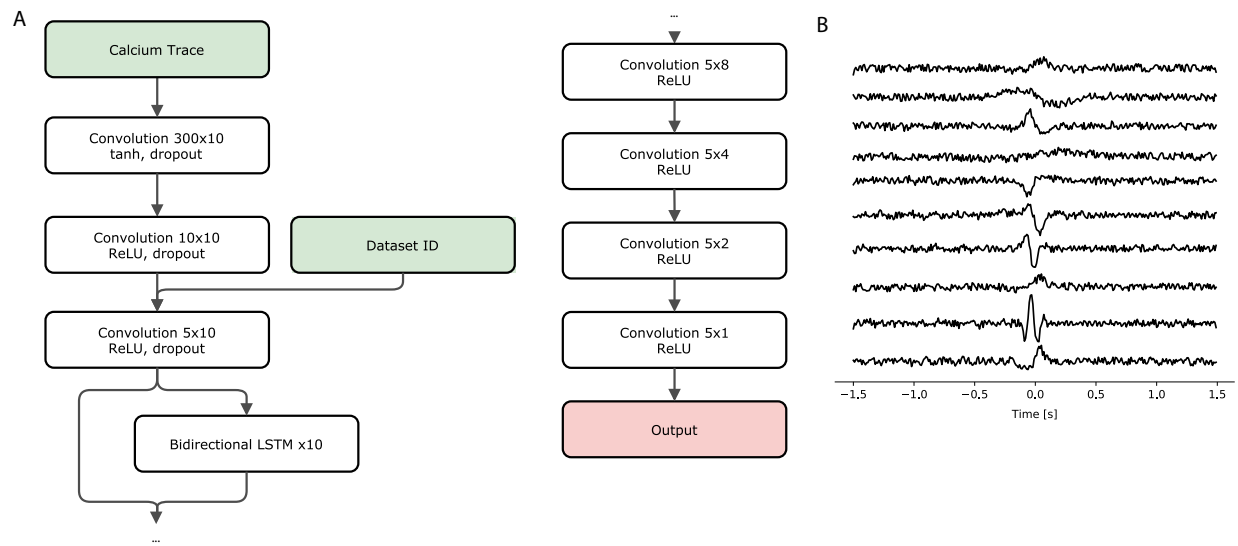


Figure 3: A. Network Architecture. In the convolutional layers the notation $m \times n$ denotes n units with kernel width of m time steps. B. Example of convolutional kernels learned by the model. The ten kernels of the first convolutional layer can describe a wide range of transient calcium dynamics.

layers with smaller kernel widths (100 and 50 ms, or 10 and 5 time steps, respectively) and with rectified linear activation functions ('ReLU'). The data set indicator is concatenated with the output of the second layer and feed into the input of the third layer. We observed that the data set indicator improved the performance of the model, possibly setting different states of the recurrent layer dynamics. Moreover, a bidirectional LSTM layer is fed by the input of the third layer, and its output is added to the input to the fourth layer. The following four layers have decreasing size, with the last layer consisting of a single unit.

To distribute the amount of information that different units are carrying, dropout is applied at the output of the first five convolutional layers.

Code is available at <https://github.com/kleskjr/spikefinder-solution>.

Team 3 — A. Speiser, S. Turaga, J. H. Macke We trained neural networks consisting both of convolutional and recurrent layers to learn a mapping from fluorescence trace to neural spiking. In contrast to other methods, we trained the network to approximate a correlated posterior conditional probability distribution $q(s|f)$ of a spike-train $s_{t=0..T}$ given a fluorescence trace $f_{t=0..T}$. We use a recurrent layer to model an autoregressive conditional probability distribution to account for correlations in this posterior between spike probabilities and previously sampled spikes, similar to ref¹⁸. The temporal ordering over spikes is used to factorize the joint distribution as $q_\phi(s|f) = \prod_t q_\phi(s_t|f, s_0, \dots, s_{t-1})$, by conditioning spike probabilities at t on all previously sampled spikes. The resulting stochastic RNN models a correlated posterior conditional distribution over spike

trains (See fig. 4). The stochastic RNN samples correlated spike trains (similar to MLSpikes) which might be useful for certain applications. However, none of the performance measures used in this challenge are sensitive to this property, as they are based on marginal firing rate predictions.

As our objective function we used the binary cross entropy between our predictions and the true spike train to train the model in a supervised fashion

$$\min_{\phi} s_t \log(q_{\phi}(s_t|f, s_0, \dots, s_{t-1})) + (1 - s_t) \log(1 - q_{\phi}(s_t|f, s_0, \dots, s_{t-1})). \quad (1)$$

In separate work¹³, we developed an approach for training this network in an unsupervised fashion using variational auto-encoders¹⁹ that can perform inference on a wide range of biophysical generative models (e.g. using the ones used by team 1). For the challenge, all available training data was labeled (i.e. ground truth spikes were provided), and we therefore trained the network using supervised learning.

Our architecture contains one forward running RNN that uses a multi-layer CNN with leaky ReLU units to extract features from the input trace. The outputs of the forward RNN and CNN are transformed into Bernoulli spike probabilities through a dense sigmoid layer. Additional input is provided by a second RNN that runs backwards and also receives input from the CNN. Forward and backward RNN have a single layer with 128 gated recurrent units each²⁰. In order to generate a single marginal probability distribution $q_{\phi}(s_t|f)$ for evaluation, samples drawn by running the stochastic RNN 50 times were averaged. We trained one separate network for each dataset.

To minimize the artifacts introduced by upsampling the data to a common imaging rate, we

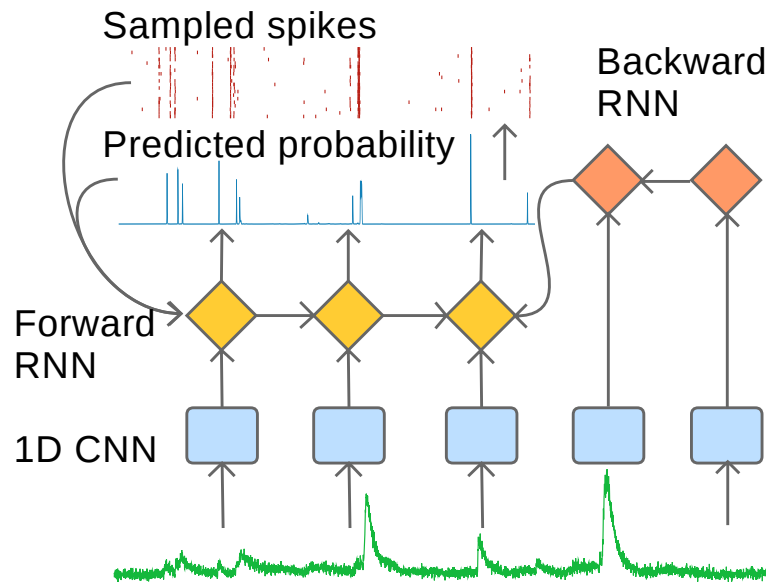


Figure 4: **Network Architecture** We use a multi-layer network architecture: Fluorescence-data is first filtered by a deep 1D convolutional network (CNN), providing input to a stochastic forward running recurrent neural network (RNN) which predicts spike-probabilities and takes previously sampled spikes as additional input. An additional deterministic RNN runs backward in time and provides further context.

performed our own pre-processing (including percentile-detrending, normalizing and resampling) where we kept the fluorescence traces as close to the original recording frequency as possible (i.e. 50, 25/3, 75, 25/2, 75 Hz for data sets 1-5 respectively). For training we split the traces into snippets of between 100-300 timesteps, using short shorter sections for lower recording rates and arranged them into batches of size 10. To cope with high firing rates which can lead to multiple spikes per time bin, predictions of our network are produced at an upsampled rate that is up to 8 times higher than the imaging rate. For the rare cases where the true spike train still contains bins with multiple spikes at this rate, we clip the values to be binary. Furthermore we used stochastic

gradient descent with the Adam optimizer (using default parameters). Each CNN layer contained ≈ 20 filters.

To find good hyperparameters we performed a small grid search on the following parameters and chose the best model using cross validation: learning rate $\{5e^{-4}, 1e^{-3}\}$, number of layers in the CNN $\{3, 4\}$, length of trace snippets $\{100, 200, 300\}$. For the upsampling-factor for superresolution, we optimized over a subset of $\{1, 2, 3, 4, 6, 8, 12\}$ depending on the dataset. Performance proved to be rather robust to the exact choice of hyperparameters. The only exception is the upsampling-factor, which needs to be sufficiently high to prevent frequent occurrence of multiple spikes per bin.

Team 4 — P. Mineault This submission casts the problem as a supervised learning problem, where the goal is to estimate the parameters of a basis transformation g and an output non-linearity h such that a loss $L(\mu_t, s_t)$ between spike train s_t and prediction μ_t is minimized. g is given by a deep convolutional artificial neural network. The first layer of this network is a standard convolutional layer followed by a rectified linear (ReLU) nonlinearity²¹, mapping each calcium time series f_t to 32 parallel time series indexed by k .

$$z_{tk}^0 = (f_t * w_{jk}^0 + \beta_k^0)^+$$

Here $(x)^+ \equiv \max(0, x)$ is the ReLU nonlinearity. We use a large window (33 time points, or 330 ms), batch normalization, as well as a dropout fraction of .3. This initial layer is followed by seven

adjustment layers in the style of a residual network²²:

$$z_{tk}^{l+1} = z_{tk}^l + \sum_m (z_{tm}^l * w_{tk}^{l+1} + \beta_k^{l+1})^+$$

These adjustment layers use smaller windows (9 time points, or 90 ms). The nonlinear component of each layer is batch normalized. Finally, the output is composed linearly via:

$$\eta_t = \sum_k z_{tk}^7 w_k^7 + \beta^7$$

The output nonlinearity h was given by a ReLU nonlinearity, such that $s_t = \eta_t^+$. We minimized a scaled sum of squared error criterion:

$$L = \sum_i \min_{\alpha_i} \frac{\sum_j (s_t^i - \alpha_i \mu_t^i)^2}{\sum_j (s_t^i)^2}$$

Here, i indexes different neurons and α_i is a set of scalars which are learned alongside the other parameters of the model (w and β). One can show that the loss is equivalent to $1 - \rho^2$, where ρ^2 is the square of the cosine similarity between prediction and spike train. The model was specified and fit using the `tf.contrib.learn` library in TensorFlow²³. Model parameters were initialized with the Xavier method and fit using the Adam optimizer. One large model for all 10 recordings from the training set was fit (173 neurons) in this phase and goodness-of-fit was monitored on a leave-aside validation set to control overfitting by early stopping. Convergence took close to 200,000 iterations.

The model described so far uses fixed filters for each recording, and uses local information (≈ 1 second of data) to estimate spikes from calcium traces. To adapt filters, we learned long-range features with an unsupervised mixture density network^{24,25}. The model, a 3-layer recursive

neural network with 512 long-short-term memory (LSTM) nodes, was fit to the calcium data to obtain one 1536-dimensional latent vector per mini-batch, which was reduced to 32 dimensions by PCA after z-scoring. These features were processed by two fully connected layers to produce 4 hidden features γ_{tp} . These 4 hidden features were used to additively adapt the filters $w_{tjk}^0 = \sum_p \text{softmax}(\gamma_{tp}) W_{jkp}$, in a manner similar to attention models.

Originally, one large model was fit for all recordings. We then created refined versions of this model for each of the 10 data sets by a transfer learning process. We took the large model with its learned parameters and ran up to 50,000 extra iterations of gradient descent on just the data from the k th dataset.

Code is available at

https://github.com/patrickmineault/spikefinder_submission

Team 5 — P. Rupprecht, S. Gerhard, R. W. Friedrich In order to infer a spike probability for time bin t (Fig. 5A), the calcium trace located around t was used, including 25% before and 75% after t , totaling to 128 samples, *i.e.*, 1.28 sec (Fig. 5C). A convolutional neural network was trained to use these 128-wide windows to predict the corresponding spiking probability. To facilitate gradient ascent, we smoothed the discrete spiking ground truth with a Gaussian filter ($\sigma = \sqrt{2}$ samples, Fig. 5B).

We implemented the convolutional neural network in Python using Keras²⁶ with the Tensorflow²³

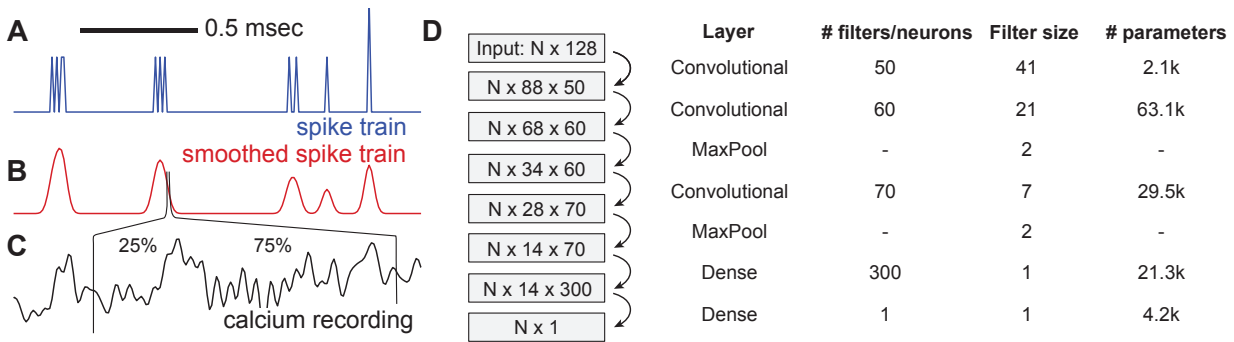


Figure 5: The basic convolutional neural network. **A,B**. The spiking ground truth was smoothed to facilitate gradient descent. **C**. A 1.28 sec time window of the calcium trace was used to infer the spiking probability for each time point. **D**. The N inputs were transformed using a neural network with three convolutional layers. The numbers in the boxes indicate the output size of the respective layers.

backend (see Fig. 5 for the network architecture). The convolutional filter size, particularly for the first layer, was chosen rather large, since simple CNNs with 3 or 4 convolutional layers with small input filter sizes (3, 5 or 7) performed poorly. No zero-padding was used. The numbers of filters were chosen to increase with depth in order to allow for a larger capacity to represent higher-order features. Standard *relu* activation units were used after each convolutional and dense layer, except for the last dense layer, where a linear activation was used to allow the output of continuous spiking probabilities.

All parameters were chosen based on intuition gained through a small exploratory hyperparameter study using diverse 3- and 4-layer CNNs with varying filter sizes, filter numbers and input window sizes. Overfitting was controlled by randomly omitting single neurons from the training

data and checking predictive performance of the CNN model for the respective omitted neuron.

Although the above-described CNN performed well when it came to fitting single datasets of the ground truth, one single model trained on all datasets usually performed not as well for any of the datasets as the same CNN trained on the respective dataset alone. To better understand this, it was quantified how well a model that had been fitted to predict spikes for neuron i can make the same kind of predictions for neuron j . To this end, a low-capacity CNN (with two locally connected convolutional layers and one dense layer) was fitted for each neuron i . The small size of the network together with a high dropout rate during training (50% after each layer) was used to prevent overfitting. This model was then applied to predict spiking probabilities both for neuron i and all neurons $j \neq i$, resulting in a matrix of 'predictive power' (measured with the Pearson correlation coefficient between prediction and ground truth, identical to the evaluation of the spikefinder competition computed (Fig. 6A). For instance, row 55 shows how well spikes of neuron 55 can be predicted by the networks generated by all other neurons. Column 55, on the other hand, shows how well the model generated by neuron 55 can predict spikes of other neurons. The 5% neurons that were worst at predicting their own spiking were discarded from the following modeling, assuming bad recording quality that is not suited for inclusion into a training dataset.

Normalization over columns, symmetrization of the matrix and averaging over datasets yields a matrix of predictive power, i.e., a matrix of proximity in prediction-space between datasets (Fig. 6B). A PCA of this matrix results in an embedding space that was limited to two dimensions due to the low number of datasets. Datasets close to each other in the embedding space (e.g. 2 and 4)

can predict each other's spikes very well, whereas datasets distant from each other in space (e.g. datasets 4 and 5) fail to do so. The idea behind this approach is very similar to the embedding spaces used by Team 8.

Using this approach, it is however not yet possible to map a neuron of a new dataset of unknown properties onto the right location of the embedding space above. To solve this problem, the following statistical properties of the raw calcium time traces were calculated (Fig. 6D), in an approach that is similar to the long-range features of calcium traces used by Team 4:

- coefficient of variation, kurtosis, skewness
- autocorrelation of the calcium time trace with its future value in 0.5, 1 and 2 seconds
- generalized Hurst exponents of order 1-5
- the power spectral density at different frequencies between 0.1 and 3.6 Hz

We did not attempt to find a minimal set of predictive properties to reduce computation time here, but used dimensional reduction techniques to automatically extract the relevant independent components. After averaging the standardized values over datasets (Fig. 6E), we used the two first principal components to generate a map of proximity in statistical property space (Fig. 6F). This map was generated using the training datasets (numbers located on the right side of the symbols). Test datasets were mapped into this PCA space (numbers on the left side of the symbols).

To generate a mapping between the locations of the datasets in the two embedding spaces,

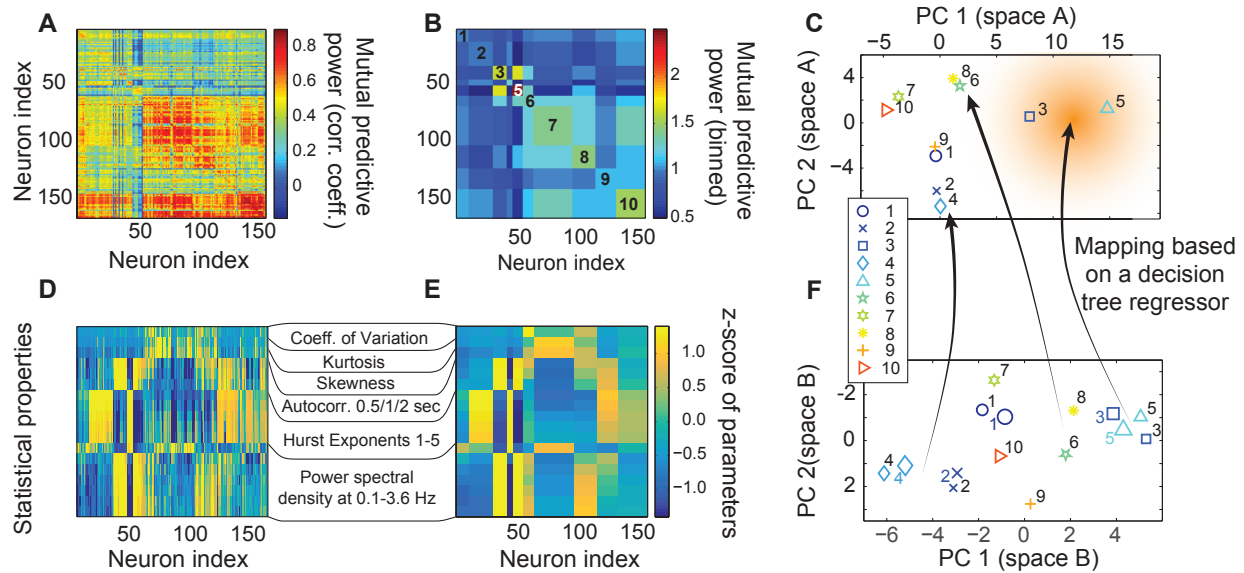


Figure 6: Using embedding spaces to choose datasets for focused retraining. **A.** Matrix of mutual predictive power, measured using the Pearson correlation coefficient between prediction and ground truth. **B.** Same as (A), but normalized for columns and binned to datasets. **C.** Principal component analysis applied to (B), keeping the first two PCs. **D.** Statistical parameters quantified for single neurons, standardized. **E.** Same as (D), but binned for datasets. **F.** 2D principal component space generated using (E). Symbols with numbers to the right are from training datasets, used to span the PCA space; symbols with numbers to the left are from the test dataset and were projected into the PCA space.

a simple regressor (*DecisionTreeRegressor* from the scikit-learn package²⁷) was fit to the training datasets (schematic arrows in Fig. 6C,F). We then used this mapping to determine the position of the test datasets in the embedding space of mutual predictive power.

Once the position in the embedding space is known for a dataset, the model that had been trained before on all datasets is retrained, but preferentially with neurons from datasets that lie close to the position in the embedding space. This preference was weighted with a function that decays exponentially over distance in the embedding space, as indicated by the red shading (Fig. 6C). Again, the functional form of the decay and the decay constant have been chosen heuristically without systematic optimization, since our goal was to showcase the power of our embedding space approach rather than finding a global optimum.

Embedding spaces as a visual and explicit intermediate step for model refinement are more easily accessible for users, allow the use of relatively small convolutional neuronal networks and can highlight similarities and differences between datasets. For example, it is interesting to see that in both embedding spaces, datasets 3 and 5 cluster together, whereas dataset 8, which uses the same calcium indicator (GCaMP6s) in the same brain region (V1), is in proximity of dataset 6 (GCaMP5k in V1). It was also observed that the datasets that use OGB-1 as indicator (1,2 and 4) tend to occupy similar regions of the embedding spaces.

This indicates that model selection is not only based on the calcium indicator and the brain region, but on hidden parameters, *e.g.*, signal-to-noise of the calcium recording, sampling rate, spike rate, temperature, indicator concentration, or others. To reliably comprise these possible

hidden parameters with embedding spaces, it will be necessary to increase the number of datasets in order to support as many possible types of datasets as possible. However, the unknown dimensionality of this hidden parameter space makes it difficult to predict how many datasets would be required.

Code is available at

<https://github.com/PTRRupprecht/Spikefinder-Elephant>.

Team 6 — J. Friedrich, L. Paninski This algorithm approximates the calcium concentration dynamics c using a stable autoregressive process of order p (AR(p)).

$$c_t = \sum_{i=1}^p \gamma_i c_{t-i} + s_t. \quad (2)$$

The observed fluorescence $\mathbf{f} \in \mathbb{R}^T$ is related to the calcium concentration as ¹¹:

$$f_t = a c_t + b + \epsilon_t, \quad \epsilon_t \sim \mathcal{N}(0, \sigma^2) \quad (3)$$

where a is a non-negative scalar, b is a scalar offset parameter, and the noise is assumed to be i.i.d. zero mean Gaussian with variance σ^2 . We assume units such that $a = 1$ without loss of generality.

The goal of calcium deconvolution is to extract an estimate \hat{s} of the neural activity s from the vector of observations \mathbf{f} . This leads to the following non-negative LASSO problem for estimating the calcium concentration^{8,11}:

$$\underset{\hat{c}, \hat{s}}{\text{minimize}} \quad \frac{1}{2} \|\mathbf{b}\mathbf{1} + \hat{c} - \mathbf{f}\|^2 + \lambda \|\hat{s}\|_1 \quad \text{subject to} \quad \hat{s}_t = \hat{c}_t - \sum_{i=1}^p \gamma_i \hat{c}_{t-i} \geq 0 \quad (4)$$

where the ℓ_1 penalty on \hat{s} enforces sparsity of the neural activity. Note that the spike signal \hat{s} is relaxed from non-negative integers to arbitrary non-negative values¹¹.

Problem (4) could be solved using generic convex program solvers, however, it is much faster to use OASIS²⁸, a dual active set method that generalizes the pool adjacent violators algorithm, a classic algorithm for isotonic regression²⁹. The dual active set method yields an exact solution of Eq. (4) for $p = 1$ and merely a greedy one for $p \geq 2$. Although an exact solution for the latter can be obtained by the primal active set method⁸, here $p = 2$ is used and the greedy but faster dual method which yielded similar scores (i.e. correlation values with ground truth).

The noise level σ is typically well estimated from the power spectral density (PSD) of \mathbf{f} ⁵. The parameters γ_i are either known a priori for a given calcium indicator or estimated from the autocovariance function of \mathbf{f} , and possibly improved by fitting them directly. The sparsity parameter λ can be chosen implicitly by inclusion of the residual sum of squares (RSS) as a hard constraint and not as a penalty term in the objective function^{5,28}. The dual problem

$$\underset{\hat{b}, \hat{c}, \hat{s}}{\text{minimize}} \quad \|\hat{s}\|_1 \quad \text{subject to} \quad \hat{s}_t = \hat{c}_t - \sum_{i=1}^p \gamma_i \hat{c}_{t-i} \geq 0 \quad \text{and} \quad \|\hat{b}\mathbf{1} + \hat{c} - \mathbf{f}\|^2 \leq \hat{\sigma}^2 T. \quad (5)$$

is solved by iterative warm-started runs of OASIS to solve Eq. (4) while adjusting λ , \hat{b} (and optionally also γ_i) between runs until Eq. (5) holds. We refer the reader to⁸ for the full algorithmic details.

The above parameter choices rely on a robust noise estimate $\hat{\sigma}$. The resampling of each spikefinder dataset to a fixed frame rate introduced artifacts into the data that corrupted the autoco-

variance and PSD such that it was not possible to obtain reliable noise and AR estimates based on the preprocessed data. Therefore, these parameters for baseline, sparsity and AR dynamics were determined based on the training data sets and kept fix for each test trace, thus not accounting for differences between neurons within one data set. Six parameters were fit: the percentile value and window length to estimate the baseline using a running percentile, the two AR coefficients, and the slope and offset of a linear function that determines the sparsity parameter λ as function of the noise. The latter was estimated on traces that were decimated by a factor of 10 to counteract the artifacts that had been introduced by upsampling the raw data.

Running OASIS with the known parameters directly yields an estimate \hat{s} of the neural activity. This estimate was already good for datasets 6-10, but noticeably improved for the first 5 datasets by convolving it with some kernel k , to obtain the final estimate $\hat{s}' = \hat{s} * k$. The kernel adjusts for mismatches between the actual calcium response kernel and the AR(2) model, smoothes the estimate, and accounts for the uncertainty of the exact spike timings by distributing spikes as spike rates over a few time bins. We used a kernel width of 30 bins and obtained it by averaging the closed form solutions of the least squares linear regression problem $k = \arg \min_k \|\hat{s} * k - s\|^2$ for each true spike train s in the training set. Interestingly, the strategy used for hyperparameter optimization used here was very similar to that used by Team 1.

Because the evaluation criterion was correlation not the residual sum of squares, we considered to further optimize the kernel for this specific criterion using gradient decent initialized at the least squares solution; however, we did not obtain significant improvements.

Code is available at

https://github.com/j-friedrich/spikefinder_submission

Team 7 — M. Pachitariu, K. D. Harris This algorithm has been developed as part of Suite2p, a complete calcium processing pipeline¹⁵. This algorithm is called L0 deconvolution and consists of solving the following problem

$$\text{minimize } \|\mathbf{f} - \mathbf{s} * k\|^2 + \lambda \|\mathbf{s}\|_0, \text{ such that } s_t \geq 0, \forall t, \quad (6)$$

where k is the calcium kernel (assumed, or estimated), $\mathbf{s} * k$ is the convolution of \mathbf{s} and k , and $\|\mathbf{s}\|_0$ is the L₀ norm of \mathbf{s} , in other words the number of non-zero entries in \mathbf{s} . We do not describe here the inference method for this model, but point the reader to our original derivation in³⁰. This solution is approximate, due to its greedy nature. Exact solutions have been obtained by³¹, in the case where the positivity constraint on \mathbf{s} was removed, and the calcium kernel was restricted to be exponential.

The L₀ deconvolution model was developed as an alternative to the L₁-deconvolution model^{5,8,11}. We originally believed that an L₀ penalty would better account for the binary nature of spike trains, and allow the algorithm to return sparse spike trains. The algorithm indeed returns very sparse descriptions of the calcium data, which can deceptively look like electrophysiologically recorded spike trains. However, neither the L₀ nor the L₁ penalties are necessary or desirable for

achieving best performance, the positivity constraint is sufficient³⁰.

Here, the training data was not used to set the parameters for the deconvolution (with the exception of time lags, see below). Instead, calcium kernels were chosen to be exponentials with timescales obtained from the literature for each specific sensor³. Following deconvolution, dataset-specific timelags were introduced for some of the spikefinder datasets. Also, the output was smoothed with a Gaussian kernel of a preset standard deviation (80ms for spikefinder data sets, 20 ms for GENIE datasets).

Code is available at <https://github.com/cortex-lab/Suite2P>.

Team 8 — B. Bolte The algorithm used for this submission consisted of a series of stacked convolutional neural networks with filter lengths of 10 to 100 milliseconds. The model was trained to maximize the Pearson correlation between the spike probabilities predicted by the model and the ground truth spike data. To capture the non-linear dynamic characteristic of this problem, additional features were added besides the raw calcium trace, including the first and second order derivatives, as well as quadratic features. Additionally, average pooling over convolutional filters was used to capture dynamics at multiple time scales.

During experimentation, it was observed that the spike behavior varied quite a bit in different data sets. From this observation, it was inferred that different convolutional filters would perform well for different data sets. To implement this idea, "data set embeddings" were used to weight

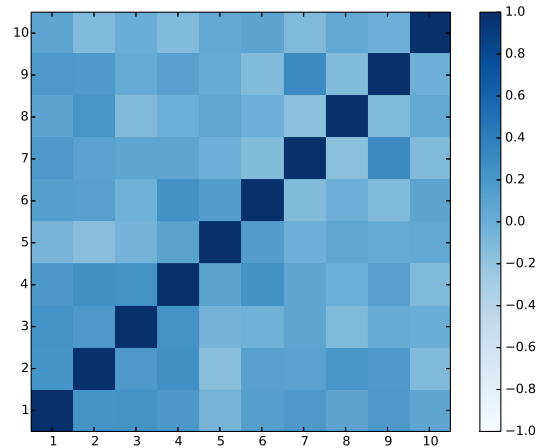


Figure 7: For each of the 10 data sets (5 spikefinder data sets and 5 GENIE-data sets), a unique embedding was learned, which was used to weight the output of the first convolutional layer of the network. Each cell represents the cosine similarity between the embeddings learned for that data set pair. A high similarity indicates that the two data sets used similar filters for inferring spike.

the output of each convolutional filter during learning. A unique vector was learned for each data set, where the number of dimensions in the vector corresponded to the number of convolutional filters in the first layer of the model. The output of the first convolutional filter was weighted by it's corresponding vector.

Intuitively, these vectors represent embeddings for each data set, and the similarity between two embeddings represents the similarity of the spike behavior in each data set, since a model trained to infer spikes in the two data set would employ similar convolutional filters. This is illustrated in Figure 7.

Code is available at <https://github.com/codekansas/spikefinder>

Team 9 — T. Machado, L. Paninski The inference framework developed by Team 9 consists of two parts: a linear encoding model that takes in spikes and outputs simulated fluorescence traces (trained on paired spike train and fluorescence data), and a simple convolutional neural network to serve as a decoding model that outputs estimates of spikes given fluorescence observations and encoding model parameter estimates. This network is trained on large data sets simulated from the encoder model. The advantage of this approach is that we can train the decoder model to “saturation” by providing it as much training data as necessary to achieve good performance. On linear-Gaussian simulated data, the neural network decoder performed comparably to OASIS⁸, a state-of-the-art inference method for efficiently solving the spike inference problem under linear-Gaussian assumptions (though both are fast enough to support online data analysis, OASIS runs significantly faster than the neural network decoder at test time).

Instead of directly using the *spikefinder* data sets to train a decoding algorithm, we generated simulated training data sets consisting of 5,000 traces, each of length 3,000 time steps. Each fluorescence trace was generated with the following second-order autoregressive model ($p = 2$):

$$c_t = \sum_{k=1}^p \gamma c_{t-k} + a s_t \quad (7)$$

$$f_t = c_t + b + \epsilon_t \quad (8)$$

The parameterization of each trace generated using Equation 8 was random. The noise was modeled as $\epsilon_t \sim N(0, \sigma_t^2)$. The jump size a of each spike was randomly sampled from a uniform distribution between 0.5 and 1.5. Each simulated spike train, s , was sampled from a homogeneous Poisson process with a mean firing rate between 0 and 2 Hz. The baseline drift component, b , was

modeled by low-pass filtering white noise. The baseline drift component significantly improved inference quality, in agreement with the observation of Team 1. In contrast, the statistics of the simulated spike trains, as well as the randomized jump sizes following each spike, had a much smaller impact on decoder performance.

The time constants of the autoregressive model, γ , and the scale of the noise, σ , were also sampled from random uniform distributions (such that a single decoder trained on these data could work well across multiple indicators and frame rates), but the precise parameterization was varied between model training sessions. However, in all cases, we found that a wide range of γ values could be learned by a single decoder model. For instance, we successfully trained decoder models across data with γ values spanning approximate decay times for fast OGB data recorded at 25 Hz, to slow GCaMP6S data recorded at 100 Hz. This shows that a single decoding model trained on simulated data can be used to analyze data produced by many different indicators and many different acquisition rates in agreement with Theis et al.⁶. Similarly, wide ranges of σ values could be learned by single decoders. However, there was a slight performance enhancement seen by training single encoders on mostly low SNR or high SNR data to improve performance on low SNR and high SNR real data, respectively.

Finally, in almost all cases, the second-order models (i.e. $p = 2$ in Equation 7) outperformed first-order models ($p = 1$). An exception were the OGB-1 data sets, as the sensor displays very rapid rise time kinetics following action potentials and has been previously shown to be especially well-described by first-order models¹¹.

To estimate the most likely spike train underlying a given fluorescence trace, we built a convolutional neural network. During training, the network was presented with f as well as parameter estimates for σ and γ given by methods published in earlier work⁵. Because the *spikefinder* data was upsampled from its native resolution and this introduced artifacts in the power spectrum of each fluorescence trace, we decimated each trace by a factor of 7-10 (depending on the approximate native time resolution of each dataset) before performing subsequent parameter fitting and analysis. The target of the network during training was the set of simulated spike trains, s , used to generate f using Equation 7.

A fairly simple architecture inspired by research into the construction of generative models for audio data was found to be effective³². In brief, the network consists of four 1D dilated convolutional layers containing 100 units, a filter size of 32, and rectified-linear (relu) nonlinearities. The first layer was dilated by a factor of 1, the second layer by 2, the third by 4 and the fourth by a factor of 8. Dropout (rate = 0.5) was also used at each layer. Finally, a fifth 1D convolutional layer with one unit, a filter size of one, and a relu nonlinearity was used to read-out a non-negative estimate of s from each f vector provided.

This architecture contained about 950,000 parameters and could be trained on a simulated data set of 5,000 traces in about 20 minutes (over 20 epochs) using the Google ML Engine. A single model trained on simulated data that spanned a wide range of σ and γ values performed well, but an ensemble of four models, each trained on a slightly different simulated data set, worked even better—as some decoders tended to work better or worse on each *spikefinder* data set. For

our submission, we chose the decoding model that worked best for each dataset to use as our submission. For data set 5, which had high firing rates, we found that convolving the results with a small Gaussian kernel resulted in a modest improvement to our inference quality.

Code is available at

<https://bitbucket.org/tamachado/encoder-decoder>

Team 10 — D. Ringach This algorithm consists of a simple linear filter followed by a static-nonlinearity $f(t) = \phi(h(t) * s(t))$. The filter $h(t)$ is a linear combination of an even filter, estimating the mean of the signal at time t , and an odd filter, estimating the derivative of the signal at time t .

The even filter is a Gaussian, $h_{even}(\tau) = A \exp(-\tau^2/2\sigma^2)$, and the odd filter is the derivative of a Gaussian $h_{odd}(\tau) = Bt \exp(-\tau^2/2\sigma^2)$. The constants A and B are such that the norm of the filters is normalized to one, $\|A\| = \|B\| = 1$. These two filters are linearly combined while keeping the norm of resulting filter equal to one, $h(\tau) = \cos \alpha h_{even}(\tau) + \sin \alpha h_{odd}(\tau)$. The output nonlinearity is a rectifier to a power, $\phi(x) = (x - \theta)^\beta$ if $x > \theta$, and zero otherwise.

The model has only 4 parameters, $\sigma, \alpha, \theta, \beta$. The amount of smoothing of the signal is controlled by σ , the shape of the filter is controlled by α , and the threshold θ and power β determine the shape of the nonlinearity. The model is fit by finding the optimal values of $\sigma, \alpha, \theta, \beta$ that maximize the correlation between its output $\hat{s}(t)$ and the recorded spiking of the neuron. Matlabs

`fminsearch` was used to perform this optimization, which was typically finished in about 60 sec or less for most data sets. The only pre-processing done was a z-scoring of the raw signals. In one dataset (dataset 5, GCaMP6s in V1), an extra-delay parameter between the signal and the prediction was allowed.

Code is available at <https://github.com/darioringach/Vanilla>.